THE ROYAL SOCIETY

X-ray topography and diffraction studies of misfit dislocation nucleation in Si-based structures

By M. S. Goorsky, P. Feichtinger, H. Fukuto and G. U'Ren

Department of Materials Science and Engineering, University of California, Los Angeles, CA 90095, USA

The combination of different X-ray topography techniques and reciprocal space mapping is used to monitor the early stages of relaxation in silicon-based heterostructures. For lightly doped silicon layers grown on heavily boron-doped 150 mm substrates, Lang transmission topography demonstrates that an orthogonal array of 60° misfits nucleates only at the wafer periphery. The length of the individual misfit segment depends on the epitaxial layer thickness and on the presence of the orthogonal blocking misfit segments. Double-crystal X-ray topography, with better strain and tilt resolution, allows one to distinguish between the different tilt components of parallel misfit dislocations. Relaxation is quantified using triple-axis X-ray diffraction. Reciprocal space maps around both the (004) and (224) reflections show that the misfits relieve about 38% of the strain. The combination of these X-ray techniques offers insight into the means to reduce dislocation formation and into the fundamental nature of the dislocations themselves.

Keywords: high resolution X-ray diffraction; topography; silicon heterostructures

1. Introduction

X-ray techniques have historically been employed in the analysis of semiconductors, and both diffraction and topography have become increasingly useful in recent years. The original applications of X-ray topography had been pioneered by the efforts of Lang and co-workers and others in the analysis of single crystals (Lang 1958; Jenkinson & Lang 1962). Lang and section topography have traditionally represented the most prominent of these techniques, with synchrotron white-beam X-ray topography (Bowen & Tanner 1992). Double-crystal reflection topography (Bonse & Kappler 1958; Koehler 1994) has also matured as a highly deformation sensitive technique for strained epitaxial layers (Petroff & Sauvage 1978; Barnett *et al.* 1995). More recently, triple-axis X-ray diffraction has emerged as a means to study defects in strained epitaxial layers through reciprocal space mapping (Koehler & Klapper 1995; Bocchi *et al.* 1997; Tanner 1999). Topographic techniques tend to provide information on a micrometre scale (limited to the grain size of the film), while diffraction typically provides information over a millimetre scale (limited to the size of the beam). Although the spatial resolution of these techniques is limited, each technique is well suited to the study of semiconductor device structures for which the effect of low-defect densities on electronic properties is very important.

 © 1999 The Royal Society

It is somewhat interesting that relatively little attention has been paid to combining these techniques to study defects in strained layer heterostructures. This combination offers information about the spatial distribution of defects and also quantifies strained layer relaxation. Although there have been several studies concerning strain relaxation in $Si_{1-x}Ge_x$ layers grown on Si, Si-based homoepitaxial layers are much more widely employed in the semiconductor industry. One example is the 'p-on-p+' structure. Here, a lightly doped (10^{15} cm^{-3}) epitaxial layer is deposited on a much more heavily doped (10^{19}–10^{20} cm^{-3}) p-type substrate. Boron is widely used as the p-type dopant and heavily boron doped silicon has a smaller lattice parameter than undoped silicon (Holloway & McCarthy 1993). The lightly doped epitaxial layer (which has the same lattice parameter as undoped silicon) is compressively strained on the p+ substrate, similar to the case of SiGe grown on silicon, and thus represents a special case of homoepitaxy which includes strain. The demand towards even more highly doped substrates dictates that strain will become an ever more important issue for this materials combination. A key issue associated with strained epitaxial layers is the ability to control strain relaxation at the interface and to determine the location, and hence the origin, of the strain-relieving defects.

Strained semiconductor layers are well known to relax by, among other mechanisms, the formation of interfacial 60° misfit dislocations (Matthews & Blakeslee 1974). Several different ideas about the origin of misfit dislocations in strained layers have been proposed. Many of these rely on the presence of pre-existing threading dislocations in the substrate (Matthews & Blakeslee 1974; Meshkinpour *et al*. 1997). Silicon substrates typically do not possess a significant concentration of threading dislocations, but the very highly doped substrates may indeed possess other defects that act as misfit dislocation nucleation sites. Other extrinsic defects, such as particulates and Ge platelets (for SiGe growth on Si), have been proposed as nucleation sites (Noel *et al*. 1993), although all of the other studies of strain relaxation in Si-based structures have focused on wafers grown by molecular beam epitaxy or low temperature vapour phase epitaxy (VPE). Very few studies have addressed the formation of defects in p-on-p+ structures, which are grown by high temperature VPE using chlorine-containing precursors and a pre-growth *in situ* etch step. Both of these factors would be anticipated to reduce the density of heterogeneous nucleation sites.

Two approaches have been reported to address the problems associated with the strain between the heavily doped p+ substrate and the lightly doped epitaxial layer. In one approach, co-doping the p+ boule with germanium had compensated the strain introduced by the high boron levels (Lin *et al*. 1991). The lattice parameter of the co-doped material is the same as undoped silicon when the germanium mole fraction is a factor of eight greater than the boron concentration. Differences in the segregation coefficients of boron and germanium in silicon dictates that uniform compensation will not be achieved throughout the length of the boule, showing that this technique does not represent a viable option for large-scale manufacturing. In another case, an oxide ring had been deposited on the substrate before epitaxial growth to block the extension of misfit dislocations, but again, this process is not commercially viable (Lee *et al*. 1994). Since neither approach is widely applicable, we have initiated a study into the origin of misfit dislocations in p-on-p+ structures and have reported on some of the mechanisms involved (Fukuto *et al*. 1999*a*, *b*). X-ray characterization figured prominently in this research programme. We focus here on these X-ray scattering techniques—Lang transmission topography, double-axis

reflection X-ray topography (DAXRT), and triple-axis X-ray diffraction (TAD)—that are employed for the study of misfit dislocations in p-on-p+ silicon structures. In the spirit of the topic for this collection of papers, we demonstrate that these techniques are increasingly valuable in addressing current materials problems in the semiconductor industry.

2. Experimental procedure

The p-on-p+ structures were grown by vapour phase epitaxy on heavily boron-doped 150 mm (001)-oriented substrates ([B] = $2\text{–}3 \times 10^{19}$ cm^{-3}). The wafers were etched using HCl/H_2 *in situ* before epitaxial growth. Trichlorosilane was used as the growth precursor and diborane as the p-type dopant ([B] $\approx 10^{15}$ cm^{-3} in the epitaxial layer) and the growth temperature was about 1100 °C. The wafer backsides were coated with a chemical vapour-deposited oxide to prevent autodoping. Layer thicknesses ranged from 2.5 to 20 µm; the 2.5 µm layer was slightly greater than the critical thickness.

Lang topography was performed using a Bede Scientific L8 camera with Mo Kα radiation (D. K. Bowen, Bede Scientific). Scanning transmission topographs of the (220) reflections from the entire 150 mm substrate were recorded using Kodak DEF5 film; a rather low resolution but high speed and high contrast film. Topographs were recorded with the diffraction vector both parallel and perpendicular to the major flat ($\langle 110 \rangle$).

DAXRT measurements were performed with a modified Bede 150 diffractometer. The first axis held a Si single crystal that can be curved to match the substrate curvature. (Koehler 1994) The crystal was miscut by 7.3° from the (001) towards a [110], providing a 1.5° angle between the incident Cu Kα radiation and the surface for the (224) reflection. This provided a beam expansion of a factor of about 40. The (224) glancing incidence reflection from a silicon reference sample produced a reflection with an intrinsic width of about 4 arc seconds; the (224) reflection was also employed here, so the diffraction vector was along a [110]. Ilford L4 emulsion plates, Kodak SR1 and Kodak DEF5 film were employed. Images were enlarged using an Olympus microscope with a CCD camera.

Reciprocal space maps were generated using a modified Bede D3 diffractometer. X-rays from a Cu point source are first diffracted through a $(+,-,-)$ series of Si (111) symmetric reflections and slits control the incident beam to a 1 mm diameter circle (which becomes an elongated footprint on the sample; the extent of the elongation depends on the reflection). The sample stage (+) and diffracted beam Si (220) analyser crystal $(-,+,-,+)$ rotate on encoded axes. A (004) reflection from a reference silicon sample produces an FWHM of 3.4 arc seconds along the ω, or rocking curve, direction and 10.0 arc seconds along $\Theta\text{–}2\Theta$.

3. Results and discussion

A key benefit associated with scanning Lang topography is the ability to measure an entire large wafer in a single measurement. Additionally, the crystallography associated with the Burgers vectors of individual dislocations can be determined (Jenkinson & Lang 1962). Lang traverse topographs show stronger diffracted intensity from distorted regions (caused by misfit dislocations, for example) than from highly perfect

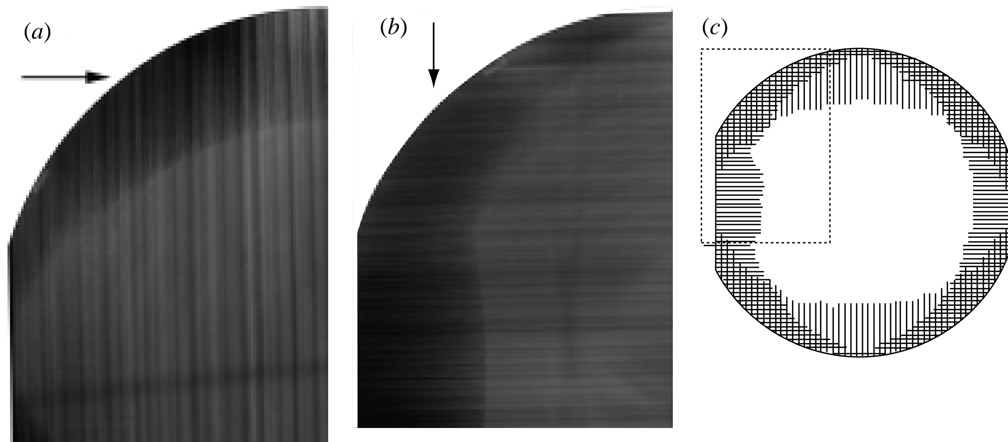

Figure 1. Lang traverse topographs from a 150 mm diameter wafer with the diffraction vector inset. The entire major flat for this wafer is shown along the lower left side. (*a*) was oriented with the diffraction vector perpendicular to the major flat. Note the misfit dislocations at the bottom left (highlighted by the arrow). (*b*) was oriented with the diffraction vector parallel to the major flat. Only one set of the pair of orthogonal misfit dislocations is visible under each condition.

regions. The higher intensity derives from the kinematical scattering associated with the regions of lower crystalline perfection, thereby allowing diffraction from a greater fraction of the initial divergent beam. A quarter portion of a full wafer Lang topograph is shown in figure 1, with the diffracted beam either parallel or perpendicular to the wafer flat. A schematic of the misfit dislocation distribution is included as well. In each diffraction case, one can observe one of the two sets of orthogonal misfit dislocations under strongly diffracting conditions, i.e. the dislocations which satisfy the $\boldsymbol{g} \cdot \boldsymbol{b}$ diffraction criterion for the different diffraction vectors (Jenkinson & Lang 1962).

There are several interesting materials issues associated with these images. First, each set of dislocations is only clearly visible under one of the diffracting conditions. The diffraction criteria support the notion that the dislocations are standard 60° dislocations along the two principal $\langle 110 \rangle$ directions. The density of dislocations in each direction is about 1500 cm^{-1} for this sample (epitaxial layer thickness is 10 μm). Second, the dislocations only appear near the wafer edge; there are no signs of nucleation, for example, at the centre of the wafer. This demonstrates that Lang topographs of large diameter wafers represent an important characterization technique for structures with low defect levels. (The slight contrast along the entire length of the wafer represents a small degree of wobble in the translation stage.) Etching measurements (Fukuto *et al.* 1999*a*) confirm that the dislocations originate at the edge, propagate towards the centre of the wafer, and terminate with a threading segment. This shows that the edge provides the only sites for dislocation nucleation under these growth conditions. The lack of misfits nucleating near the centre of the wafer demonstrates that the substrate does not possess a high density of suitable bulk defects and that the high temperatures and Cl-containing ambient associated with VPE growth minimize the density of surface particulates. Only the crystalline imperfections associated with the edge of the wafer are available as suitable nucleation sites. Third, a front of

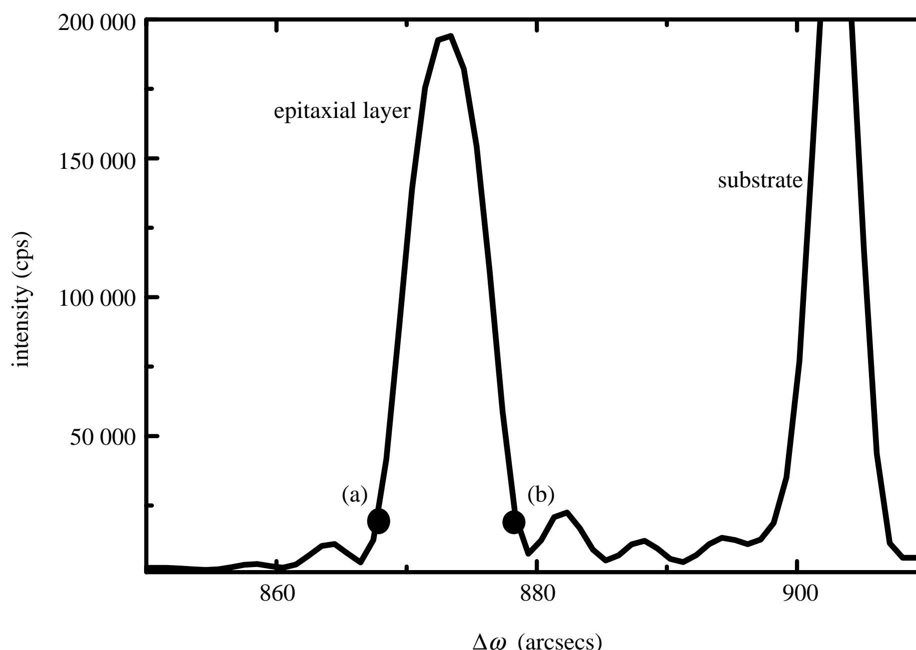

Figure 2. (224) glancing incidence rocking curve from wafer with 2.5 μm epitaxial layer with 'working points' for topographic images in figure 3 marked as (*a*) and (*b*).

dislocations extending from the edge is clearly visible, but there are also dislocations that have lengths that are measurably shorter. This indicates that the dislocations nucleate at different times during growth. Layers grown for longer times (and correspondingly greater thicknesses) possess commensurately longer dislocations (Fukuto *et al*. 1999*b*). A fourth observation is that the misfit dislocations are longer if there are fewer interactions with orthogonal dislocations. This is observed most clearly near the wafer flat, which is at the bottom of the images in figure 1. There are few orthogonal dislocations (parallel to the flat) and the dislocations perpendicular to the flat are indeed longer than they are at positions where a significant density of orthogonal dislocations exists. These results are consistent with the findings of Gillard *et al*. (1994), who showed that strain fields associated with the orthogonal set of dislocations can act to block or impede the lengthening of the misfit segments.

The results from the Lang topography are highly enlightening in terms of the dislocation nucleation sites, but more strain sensitive techniques can provide further information. DAXRT, which offers such sensitivity to both strain and tilt in the lattice, has greater potential to assess the properties of the misfit segments. One specific form of DAXRT is that of 'weak beam' topography in which the diffracted image is obtained from the wings of the diffraction peak. At these positions far from the Bragg condition, the primary sources of diffracted intensity are the defect regions. Petroff *et al*. (1980) employed this technique using a synchrotron source and reflection geometry. They demonstrated that the images from misfit dislocations exhibited either 'white' or 'black' contrast under weak beam conditions. However, significant curvature present in the layers complicated the analysis of the diffraction vectors.

Our DAXRT measurements using the curved crystal collimator and a sealed tube X-ray source show similar information as had been observed with the synchrotron. The results presented here are from a wafer with a 2.5 μm epitaxial layer. The topographs were taken at different working points of the epitaxial layer diffraction peak; the rocking curve for this peak is shown in figure 2 with the working points marked (at *ca.* 10% of the maximum intensity on either side of the peak, the above-mentioned weak beam case). One benefit associated with DAXRT using a curved first crystal is the uniform illumination of curved samples In comparison with the early work of Petroff *et al.* (1980), where curvature led to changes in the Bragg angle across the topographic image, the curved crystal helps maintain a constant Bragg angle over the imaged area. This simplifies the interpretation of the diffraction contrast in the image.

Figure 3*a* shows a topograph taken from near the edge of the wafer. This 'weak beam' image is recorded at the high angle side of the (224) diffraction peak. The misfit segments that are parallel to the diffraction vector show up as faintly higher intensity than the background of the substrate. Interestingly, the dislocations that are perpendicular to the diffraction vector show up either as strong white lines or as black lines (or at least as dark lines which diffract much less than the surrounding Si matrix). In all cases, the dislocations remain the same intensity along their entire length, indicating that pinning (Tanner *et al.* 1997) is not occurring and that the dislocations remain at the strained-layer–substrate interface. It is also clear that there is a difference in the number of these black/white dislocations in this area.

Figure 3*b* depicts the topograph from the same location at the low-angle side of the rocking curve. Here, the parallel (to the diffraction vector) dislocations exhibit a slightly different level of contrast as before (darker than the substrate), although the three observed dislocations exhibit the same contrast as each other. The contrast associated with the individual perpendicular dislocations, however, is completely reversed. The dislocations that showed high intensity under the previous orientation, now show lower intensity than the matrix. This confirms that there are two types of distinguishable dislocations along a given $\langle 110 \rangle$ direction. Furthermore, rotating the diffraction vector by 90° confirms that the contrast between the 'parallel' and 'perpendicular' switches sense: the former become white/black (in fact, each of the three dislocations again possesses the same contrast) and the latter become 'grey'.

The change in contrast for each of the two sets of orthogonal dislocations can be described in terms of the different components associated with misfit dislocations. A family of 60° dislocations in the [110] have Burgers vectors that can be described in terms of their misfit, screw, and tilt components, respectively. Consider the parallel pair of misfit segments which extend along the [110]; the Burgers vectors include the $\frac{1}{2}[101]$ and the $\frac{1}{2}[0\bar{1}1]$:

$$\tfrac{1}{2}[101] = \tfrac{1}{4}[1\bar{1}0] + \tfrac{1}{4}[110] + \tfrac{1}{2}[001], \tag{3.1 a}$$

$$\tfrac{1}{2}[0\bar{1}1] = \tfrac{1}{4}[1\bar{1}0] + \tfrac{1}{4}[\bar{1}\bar{1}0] + \tfrac{1}{2}[00\bar{1}]. \tag{3.1 b}$$

In this case, they possess the same misfit-relieving component, but have opposite screw and opposite tilt components. The strong black/white contrast from the dislocations that are perpendicular to the diffraction vector stems from the different tilt components associated with each of the dislocations, and is consistent with simulated images (Spirkl *et al.* 1994). This confirms that the tilt component of individual misfit dislocations can be determined using DAXRT using a standard laboratory source

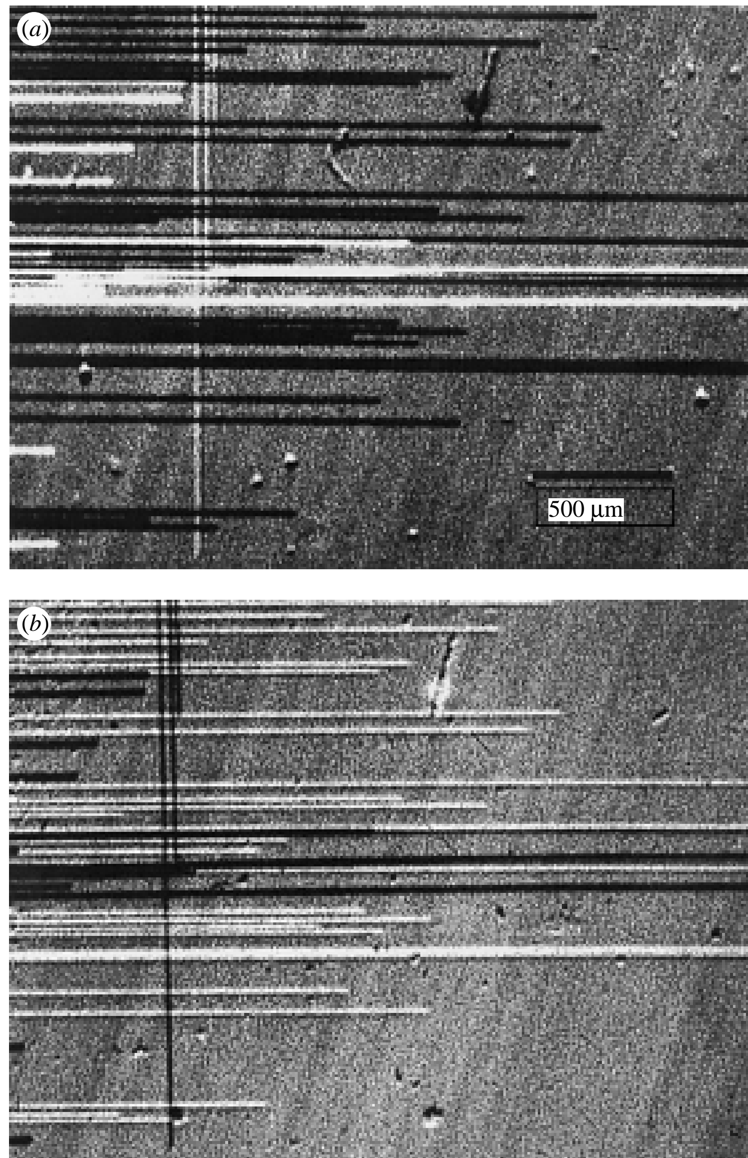

Figure 3. (224) glancing incidence topographs: (*a*) taken at position (a) in figure 2, showing individual misfit dislocations with either black or white contrast (the diffraction vector is along the vertical direction). (*b*) taken at position (b) in figure 2 shows the reversal in contrast associated with the different tilt components of the misfit dislocations that are perpendicular to the diffraction vector.

(Petroff *et al*. 1980). This determination, without requiring defect image simulation, allows a direct means of quantifying the properties (density, velocity, etc.) of each of the different dislocation types (P. Feichtinger and others, unpublished work). For example, the difference in the density of the two types of dislocations indicates that the nucleation mechanisms for each is different; this is a topic of current investigation.

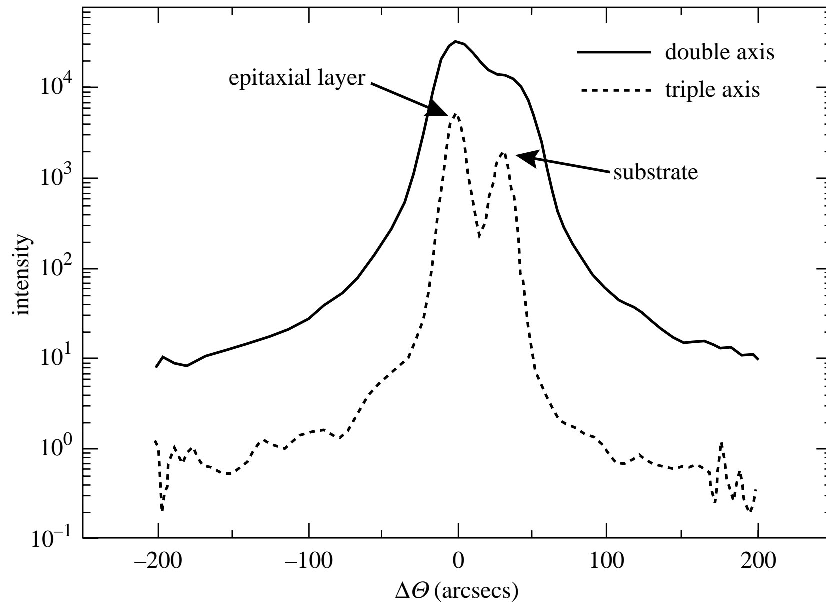

Figure 4. Double- and triple-axis Θ–2Θ scans of the epitaxial layer and substrate peaks.

Likewise, dislocations parallel to the diffraction vector in figure 3 also show contrast compared with the perfect silicon. For these dislocations, it is their screw components that possess the correct Burgers vector to produce an image. The magnitude of the effect is expected to be smaller than for the tilt component (the Burgers vector for the screw component is smaller than the Burgers vector associated with the tilt, e.g. equation (3.1)) as is observed here, but the contrast also changes with a 180° change in the diffraction vector direction. These results demonstrate that the Burgers vector components of each pair of the orthogonal misfit segments can be determined.

The presence of misfit dislocations suggests that relaxation may be occurring, although the topographs themselves do not provide for a straightforward means of quantifying the residual strain present in the layers. Double- or triple-axis diffraction measurements are better suited for this purpose. The layers are relatively thick, and although only slightly strained, will introduce curvature to the lattice and thus broaden the double-axis diffraction rocking curves. Figure 4 compares the double-axis and triple-axis Θ–2Θ scans from a structure with a 20 μm thick epitaxial layer taken near the centre of the wafer (away from the misfit dislocations). The difference in position between the substrate and epitaxial layer peaks is somewhat obscured in the double-axis measurement, indicating that a strain analysis would be obscured by materials issues. The diffraction peaks in the TAD scan are much more narrow, demonstrating that the broadening observed in the double-axis diffraction measurement stems from lattice curvature. In the area of the wafers where there are no dislocations present, absolute lattice parameter measurements (Yoon *et al*. 1997) show that the (001) substrate lattice parameter is 5.4303 Å, which corresponds to a boron concentration of 2.6×10^{19} cm^{-3} and induces a strain in the layer, $\varepsilon = 1.5 \times 10^{-4}$. The layer perpendicular lattice parameter is greater than that of undoped silicon (5.4322 Å versus 5.4310 Å), indicating that the layer is under biaxial compression, as in the case of SiGe deposited on lightly doped silicon.

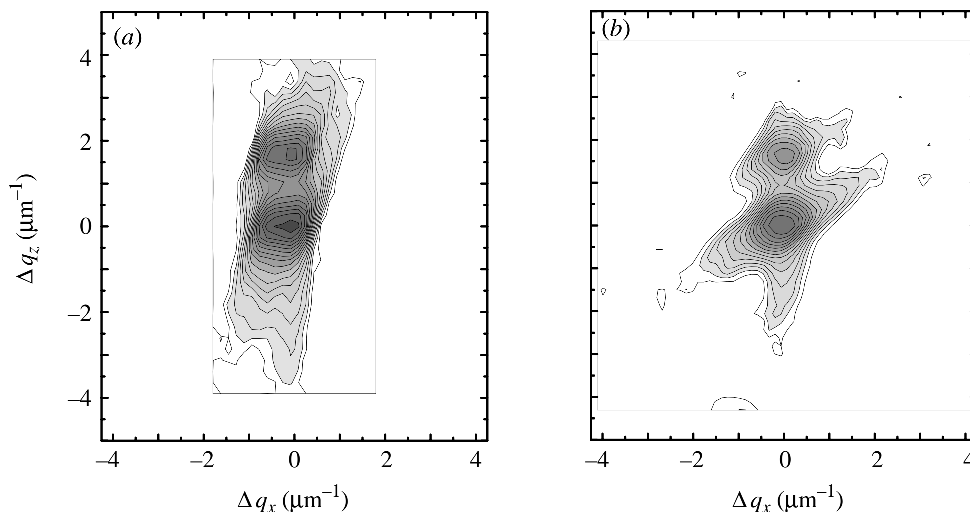

Figure 5. (*a*) shows the (004) reciprocal space map at a position without misfit directions. (*b*) shows the corresponding (224) reflection at the same position. The grey log intensity scale ranges from 1 count per second (cps) to 4000 cps.

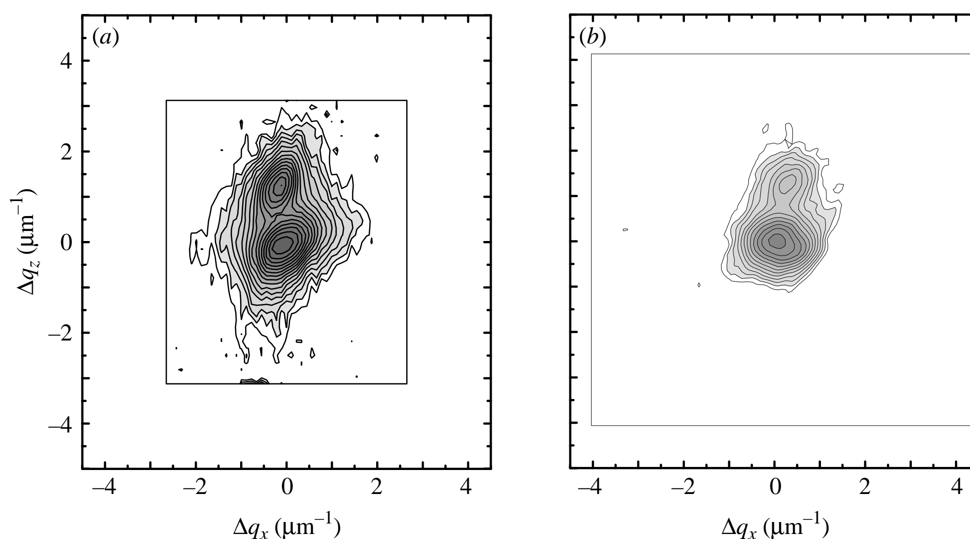

Figure 6. (*a*) shows the (004) reciprocal space map from a region near the edge of the substrate that included misfit directions. (*b*) shows the corresponding (224) reflection. The intensity scale is the same as in figure 5.

Reciprocal space maps around the (004) and (224) reflections for the same 20 µm epitaxial layer structure (figure 4) help to quantify the modifications to the strain state of the layer due to the dislocations. Near the centre of the wafer, the (004) reflection space map shows (figure 5*a*) that the layer and substrate peaks lie on the same vertical axis. This demonstrates that there is no measurable tilt between the substrate and layer. The (224) space map (figure 5*b*) from this same region shows

that there is no additional displacement between the two peaks. This confirms that the substrate and layer possess the same in-plane lattice parameter; in other words, the layer is pseudo-morphic. Figure 6 shows the reciprocal space maps from a region near the edge of the structure, where the misfit segments are present. Relaxation is observed most clearly here through the shift of the position of the in-plane (224) epitaxial layer position compared with that of the substrate positions. There is also greater broadening of both the substrate and the layer peaks, consistent with the presence of dislocations at the interface (Goorsky *et al*. 1995). Converting the shift in reciprocal space to a measure of relaxation indicates that the layer is *ca.* 39% (with an error of *ca.* $\pm 2\%$) relaxed. The resolution associated with the triple-axis diffraction measurements provides a means to determine the extent of relaxation in these structures, whereas the double-axis measurements (e.g. figure 4) do not clearly distinguish between the layer and substrate peaks. Using this information, one can relate the measured relaxation with the dislocation density. If the degree of relaxation is greater than that which could be produced by the misfit density, other factors must also contribute to the relaxation (Chu *et al*. 1985).

The misfit dislocation density for this sample is only *ca.* $2 \times 10^3\ \text{cm}^{-1}$. However, the strain in this sample is also quite low ($\varepsilon = 1.5 \times 10^{-4}$) so this dislocation density would be expected to produce a relaxation of 37% ($\pm 2\%$, also). This value matches that obtained from the reciprocal space maps. In other words, the measured strain relaxation is fully accounted for by the misfit dislocations. Therefore, the topographs show all of the defects, which are responsible for the lattice relaxation, and the TAD measurements quantify the extent of relaxation.

Moving the incident beam further from the wafer edge (where the dislocation density is lower) leads to a reduced relaxation (Fukuto *et al*. 1999*a*) as expected. Rotating the sample changes the diffraction condition and allows determination of the lattice parameter along both $\langle 110 \rangle$ directions. In some regions (e.g. near the wafer flats) there were only dislocations along one of the two orthogonal directions, and the reciprocal space maps confirm that the layer is pseudo-morphic along this direction. Therefore, a deviation from the tetragonally distorted lattice can be detected (no measurable tilts were observed) which evolves towards a tetragonal distortion towards the centre of the wafer.

4. Conclusions

The Lang topography technique and DAXRT and TAD combine to provide non-destructive means to determine the relaxation mechanisms in silicon p-on-p+ epitaxial structures. The Lang technique proved to be extremely useful to determine the origin of misfit segments and also provided some information about the Burgers vectors associated with them. In this application, the Lang topographs clearly showed that the misfit segments nucleated at the periphery of the wafers. DAXRT provides much higher strain and tilt resolution; this combination has been applied here to demonstrate that different types of parallel dislocations can be distinguished by the components of their Burgers vectors while using a standard laboratory source. TAD measures the extent of relaxation, tilt, and composition in these strained heterostructures. This combination of techniques is particularly well suited to systems with low dislocation densities and provides important information about defect formation in strained silicon-based epitaxial systems.

This work was supported through the UC MICRO Program and Wacker Siltronic Corp. (Portland, OR) and the National Science Foundation (95-02117).

References

Barnett, S. J. (and 16 others) 1995 *In situ* X-ray topography studies during the molecular beam epitaxy growth of InGaAs on (001) GaAs: effects of substrate dislocation distribution on strain relaxation. *J. Phys.* D **28**, A17–22.

Bocchi, C., Ferrari, C., Lagomarsino, S. & Tapfer, L. (eds) 1997 *Proc. XTOP Conf. Nuovo Cim.* **19**.

Bonse, U. & Kappler, E. 1958 Roentgenographische Abbildung des Verzerrungsfeldes einzelner Versetzungen in Germanium–Einkristallen. *Z. Naturforsch.* A **13**, 348–349.

Bowen, D. K. & Tanner, B. K. 1992 Synchrotron X-radiation topography. *Mater. Sci. Rep.* **8**, 369–407.

Chu, S. N. G., Macrander, A. T., Stege, K. E. & Johnson, W. D. 1985 Misfit stress in InGaAs/InP heteroepitaxial structures grown by vapor-phase epitaxy. *J. Appl. Phys.* **57**, 249–257.

Fukuto, H., Feichtinger, P., Goorsky, M. S., Magee, T., Oster, D. & Moreland, J. 1999*a* Structural defects in p/p+ vapor phase epitaxy. *Proc. 1999 Electrochemical Society Spring Meeting.* Pennington, NJ: The Electrochemical Society.

Fukuto, H., Feichtinger, P., U'Ren, G. D., Lindo, S., Goorsky, M. S., Magee, T., Oster, D. & Moreland, J. 1999*b* Misfit dislocation formation in p/p+ silicon vapor phase epitaxy. *J. Crystal Growth.* (In the press.)

Gillard, V. T., Nix, W. D. & Freund, L. B. 1994 Role of dislocation blocking in limiting strain relaxation in heteroepitaxial films. *J. Appl. Phys.* **76**, 7280–7287.

Goorsky, M. S., Meshkinpour, M., Streit, D. C. & Block, T. R. 1995 Diffuse X-ray scattering from misfit dislocations at semiconductor hetero-interfaces. *J. Phys.* D **28**, A92–A96.

Holloway, H. & McCarthy, S. L. 1993 Determination of the lattice contraction of boron-doped silicon. *J. Appl. Phys.* **73**, 103–110.

Jenkinson, A. E. & Lang, A. R. 1962 X-ray diffraction topographic studies of dislocations in floating-zone grown silicon. In *Direct observation of imperfections in crystals* (ed. J. B. Newkirk & J. H. Wernick), pp. 471–495. New York: Wiley Interscience.

Koehler, R. 1994 High-resolution X-ray topography. *Appl. Phys.* A **58**, 149–157.

Koehler, R. & Klapper, H. (eds) 1995 *Proc. XTOP Conf. J. Phys.* D **28**, no. 4A.

Lang, A. R. 1958 Direct observation of individual dislocations by X-ray diffraction. *J. Appl. Phys.* **29**, 597–598.

Lee, H.-J., Kim, C.-S., Han, C.-H. & Kim, C.-K. 1994 Direct growing of lightly doped epitaxial silicon without misfit dislocation on heavily boron-doped silicon layer. *Appl. Phys. Lett.* **65**, 2139–2141.

Lin, W., Hill, D. W., Paulnack, C. L., Kelly, M. J. & Benson, K. E. 1991 Misfit stress and dislocations in p/p+ epitaxial silicon wafers: effect and elimination. In *Defects in silicon II* (ed. W. M. Bullis & U. Goesele), pp. 163–171. Pennington, NJ: The Electrochemical Society.

Matthews, J. W. & Blakeslee, A. E. 1974 Defects in epitaxial multilayers. *J. Crystal Growth* **27**, 118–125.

Meshkinpour, M., Goorsky, M. S., Jenichen, B., Streit, D. C. & Block, T. R. 1997 The role of substrate quality on misfit dislocation formation in pseudomorphic high electron mobility transistor structures. *J. Appl. Phys.* **81**, 3124–3128.

Noel, J. P., Rowell, N. L., Houghton, D. C., Wang, A. & Perovic, D. D. 1993 Phonon-resolved and broad photoluminescence in strained Si_{1-x}/Ge_x/alloy MBE layers. *J. Electron. Mater.* **22**, 739–743.

Petroff, J. F. & Sauvage, M. 1978 Misfit dislocation characteristics in quaternary heterojunctions $Ga_{1-x}/Al_x/As_{1-y}/P_y$/GaAs analysed by synchrotron radiation white beam topography. *J. Cryst. Growth* **43**, 628–636.

Petroff, J. F., Sauvage, M., Riglet, P. & Hashizume, H. 1980 Synchrotron-radiation plane-wave topograhy. I. Application to misfit dislocation imaging in III–V heterojunctions. *Phil. Mag.* **42**, 319–338.

Spirkl, W. (and 11 others) 1994 Simulation of X-ray reflection topographs from misfit dislocations. *Phil. Mag.* **69**, 221–236.

Tanner, B. K. (ed.) 1999 *Proc. XTOP Conf. J. Phys.* D **32**, no. 10A.

Tanner, B. K., Moeck, P. & Mizuno, K. 1997 Identification of misfit dislocations using X-ray scattering and topography. *Inst. Phys. Conf. Ser.* **160**, 177–186.

Yoon, H., Lindo, S. E. & Goorsky, M. S. 1997 Characterization of ternary substrate materials using triple axis X-ray diffraction. *J. Crystal Growth* **174**, 775–782.